WCTE 2014 Quebec City Canada August 10-14
World Conference on Timber Engineering

A FORM FINDING METHOD FOR POST FORMED TIMBER GRID SHELL STRUCTURES

Bernardino D'Amico[1], Abdy Kermani[2], Hexin Zhang[3]

ABSTRACT: Timber grid shells provide efficient ways of covering large openings with relatively small amount of materials. With three-dimensional CAD software, it is now possible to model a free-form surface and discretize it in smaller straight elements, thus postponing the design of the node-connections geometry to the manufacturing process (i.e. by Computer-Aided-Manufacturing). A "low-tech" method for building free-form timber grid shell structures with standardized connections is that of assembling an initially flat grid of continuous rods and then, post-forming (bending) it in a double curved shape. Accordingly, the latter method doesn't require high-tech manufacturing processes. However, being the final shape influenced by equilibrium of the internal forces, a form-finding procedure is required. A novel "facilitating" numerical framework is introduced in this paper: For a given continuous reference shape, a geometrically similar discrete model is found by implementation of a six degree of freedom formulation of the Dynamic Relaxation method. Numerical methods to the finding of grid cutting pattern, as well as, a Newton-Raphson method to assess the allowable timber cross-section, are illustrated. The theory is validated by numerical examples of a single-rod case and a corrugated barrel vault.

KEYWORDS: Free-form structures, Grid shell, Solid wood, Form-finding, Parametric design, Dynamic Relaxation, Newton-Raphson.

1 INTRODUCTION

A grid shell is a structure that gains its strength and stiffness through its double curvature configuration. Its advantages are a minimum use of materials, structural efficiency and the creation of a large volume, as well as the potential for quick and cost-effective construction, (Harris et al. [1]). Form-resistant grid shell shapes can be realized by connecting short straight beam elements together into nodes so discretizing the curved surface to a facetted shell or bending initially flat elastic rods such as solid timber planks/laths obtaining thus real continuous curves. For this second case, two sub-categories can be defined [1] differentiating on the geometric parameters assigned to generate a grid onto a continuous surface: If screwed laminated timber ribs are arranged following geodesic patterns (shortest curve onto a surface for two given points) the planks composing the rods will only be subjected to torsion and bending around the weak axis [2] (e.g. Hanover Expo Canopy, 2000 by Julius Natterer) enhancing the allowable width of the cross-section of the planks. A different approach was adopted in the design of the Mannheim timber grid shell for the Garden Festival [3]. In this case, it was assumed a constant distance between consecutive nodes of the same rib (composed by two overlapping timber laths). According to Pirrazzi et al. [2] the resulting (Chebyshev net) geometry of the grid shell did not follow the geodesic paths. However, this second design approach allowed the possibility of assembling the grid shell laid out flat and eventually "post-forming" it in a double curved geometry by imposing external displacements under the form of temporary crane/cable systems or adjustable scaffolding [4-6]. Since the construction of the Mannheim grid shell, this technique only rarely has been used. According to Kelly et al: *"The reason for the apparent lack of enthusiasm may stem from the unique challenges associated with the design and formation process"* [7]. In fact, in order to draw out the post-formed grid shape (and gain information on internal stress field) a form finding analysis with large displacements formulation is required to simulate the curvature formation process. Regardless of the adopted numerical method, the form finding will requires the definition of initial parameters to be performed, such as the cutting pattern geometry of the flat grid and external imposed displacements magnitude and direction. To

[1] Bernardino D'Amico, Centre for Timber Engineering (CTE), Edinburgh Napier University, 10 Colinton Road, Edinburgh, UK. Email: b.d'amico@napier.ac.uk Canada.
[2] Prof. Abdy Kermani, director of CTE, Edinburgh Napier University, 10 Colinton Road, Edinburgh, UK. Email: a.kermani@napier.ac.uk
[3] Dr. Hexin Zhang, School of Engineering & the Built Environment, Edinburgh Napier University, 10 Colinton Road, Edinburgh, UK. Email: j.zhang@napier.ac.uk

facilitate the design process of post-formed grid shells, a form finding method is introduced in this paper.

2 METHOD

Different authors [6, 8-12] addressed the problem of defining numerical methods to speeding up the design process of post formed grid shells: An interesting concept coming out is that of using a supporting (reference) surface on which the mat is "forced" to bend. Generally, the method contemplates two consecutive steps:

- A flat two-way mesh is pulled on the reference surface by means of external axial springs [11] or external applied forces [9]. Alternatively, the mesh is constrained to slide on the surface.
- With the equilibrium shape eventually found, the mesh geometry exceeding the reference surface is deleted [9] (a cutting pattern is thus found) and degrees of freedom (DoF) of the boundary nodes are constrained while the previous external forces (or springs) are disabled (released). Accordingly, the system assumes its final equilibrium configuration.

Clearly, a two-step analysis scheme allows finding the equilibrium shape close to a reference surface which can be modelled in accordance to a wide range of design requirements: Harris et al explained how architectural and regulation parameters were driving the shape of the Pods grid shell roof and only in a second design phase *"...a number of trials were made to establish a grid onto a surface"* [13].

Figure 1: *Post-formed timber grid shells* [12].

2.1 TIMBER CROSS SECTION AND CURVATURE

The internal stresses generated for the effect of post forming process, restricts to a certain domain the size of the lath's cross-section. For this reason, a method for automatic assessment of the "allowable" laths thickness is proposed in this work.

3 THEORY

3.1 Dynamic Relaxation method

In order to handle the large displacements involved in the forming process, a suitable numerical method is required: An *ad-hoc* formulation of the Dynamic Relaxation (DR) method has been developed for this specific case. The DR is a fictitious time increment marching scheme where, the position of the nodes representing the structural system is obtained by numerical integration of the Newton's second law of motion until the entire system settles down in a static equilibrium by application of a viscous or kinetic damping term. The method, independently proposed by Day [14] and Otter [15], has been extensively used for a wide range of non-linear structural problems as for instance, the form finding and load analysis of tension structures where it leads to more reliable results in terms of solution convergence if compared with much known matrix schemes with Newton-Raphson solver [16]. The method is (in general) implemented by considering three translational DoF per node, thus only allowing simulation of able/strut behaviour-like. However, it has been proven that three DoF schemes can efficiently takes into account bending [17] and torsion [18] member stiffness if identical moments of area around any axis of the element cross-section are given. In general, this is not the case of post formed timber grid shells, where rectangular cross-section may be used. For this reason, a more comprehensive six DoF scheme per node (three translational DoF plus three rotational DoF) has been developed: Assuming the discrete mesh geometry represented by a set $\{P\}$ of nodes:

$$\{P\} = \{\bar{r}_i \ldots \bar{r}_n\} \quad ; \quad \bar{r}_i = [x \quad y \quad z] \tag{1}$$

With x, y, and z being the coordinate values in the (global) reference system of the ith node, and a connectivity (element) list storing the node's indexes of the element ends (1, 2):

$$\{N\} = \{n_j \ldots n_n\} \quad ; \quad n_j = \{i_1, i_2\} \tag{2}$$

The rotational DoF are taken into account by assuming, for the ith node, a local coordinate system of unit vectors:

$$\{\bar{x}_i, \bar{y}_i, \bar{z}_i\} \tag{3}$$

With z_i the tangent direction to the rod's longitudinal axis and x_i, y_i the cross-sectional axes. In addition to the nodal

lumped masses (m_i) needed to compute the displacements, rotational masses (moment of inertia j_i) are taken into account, in order to compute the rotational angles of the local system. At each DR time step, the nodal position and local system orientation at time *t* are used to compute the corresponding residual (out of balance) forces $\overline{R}_i^t$ and moments $\overline{H}_i^t$ acting at the *i*th node for effect of the surrounding elements internal reactions. Thus, the updated nodal coordinate and local system orientation at time $t + \Delta t$ are obtained by numerical integration of the linear acceleration terms $\ddot{x}_i^t, \ddot{y}_i^t, \ddot{z}_i^t$ and angular accelerations terms $\ddot{\vartheta}_{i,x}^t, \ddot{\vartheta}_{i,y}^t, \ddot{\vartheta}_{i,z}^t$ around the global *x*, *y* and *z* axes:

$$\ddot{x}_i^t = \frac{R_{i,x}^t}{m_i} \quad ; \quad \ddot{\vartheta}_{i,x}^t = \frac{H_{i,x}^t}{j_i} \tag{4}$$

3.2 Modelling cylindrical hinges

In order to apply the DR method for a two-way grid shell system, the kinematic of the nodal connection needs to be properly modelled. For a double layer grid shell, standard connections such as slotted-hole (Figure 2-a) or clamping plate systems may be provided. Alternatively, only one grid layer is pre-assembled and formed, thus the second layer screwed on a second construction phase. In any case, a hinge mechanism occurs at the nodal connections of the two-way mat.

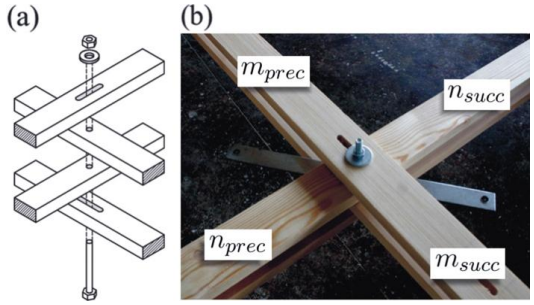

Figure 2: *Slotted-hole connection system: (a) Schematic view; (b) Two distinct {N} and {M} connectivity lists are used to define the equivalent numerical model.*

In general such hinge-like connections are (numerically) modelled by placing the mesh elements on two staggered levels and connecting them by means of *link* elements which allow rotation around their longitudinal axis. Although faithful to the real geometry, doubling the mesh nodes at each connection generates local eccentricities. On the contrary, a "simpler" model with only one node per connection is numerically more stable. This can be achieved by assuming a double connectivity list (for instance {N} and {M}) thus having a list for each direction of the mesh (Figure 2-b) and a second local coordinate system such that each connection is defined by a single position vector (Eq. 1) but two local systems:

$$\left\{\bar{x}_{i,n}, \bar{y}_{i,n}, \bar{z}_{i,n}\right\} \quad ; \quad \left\{\bar{x}_{i,m}, \bar{y}_{i,m}, \bar{z}_{i,m}\right\} \tag{5}$$

3.3 Surface constraints

Fundamental requirement for the initial nodes position is obviously that they have to lie on the reference surface. Assuming such surface described by a *real* function of the kind $f(x, y, z) = 0$ with the function's arguments corresponding to the nodal coordinates (Eq. (1)):

$$\{P\} \subset \{x, y, z \mid f(x, y, z) = 0\} \tag{6}$$

In addition, we have to define a "subspace of interest" of the Cartesian space containing the part of mesh (a subset of $\{P\}$) that we want constrained to slide in the surface. Indicating with *B* the subspace of interest, the following condition applies:

$$\forall \bar{r}_i \in B \Rightarrow \overline{R}_i^t = \overline{R}_{i,\parallel} = \overline{\omega}_i \times (\overline{R}_i \times \overline{\omega}_i) \tag{7}$$

At each DR iteration, the node set *P* is entirely traversed to check whether condition (7) applies: If $\bar{r}_i \notin B$ thus, the residual force $\overline{R}_i$ is inserted in Eq. (4) to eventually obtain the updated node position, otherwise; only the component tangent to the surface $\overline{R}_{i,\parallel}$ is used to compute the acceleration term.

3.4 Mesh cutting

Once the elastic grid constrained to the surface reaches a static equilibrium configuration, at completion of the first DR analysis step, the mesh geometry is initialized for the second DR analysis step by "cutting" the excess part. This task is performed by interrogating the connectivity lists $\{N\}$ and $\{M\}$ checking, for each element, whether the corresponding end nodes fall into *B*. In case both end-nodes are outside the subspace of interest, the element is discharged from the connectivity list. However, if the element crosses the subspace with one of its end nodes, manipulation of the geometry list $\{P\}$ is required: Let assume that *B* is lower bonded by $z \geq 0$ and $\bar{r}(t)$ is the cubic *Hermite* shape function of the crossing element, defined by the end nodes coordinate $(\bar{r}_{i_1}; \bar{r}_{i_2})$ and tangent unit vectors $(\bar{z}_1; \bar{z}_2)$. The problem is reduced to find the value of t_0 such that $\bar{r}(t_0)$ lies on the global (*x*, *y*) plane:

$$t_0 \rightarrow \bar{r}(t_0) = [x \quad y \quad 0] \quad ; \quad t_0 \in [0,1] \tag{8}$$

Hence, we take into account only the third component of Eq. (8):

$$t_0 \rightarrow z(t_0) = 0 \tag{9}$$

This can be iteratively solved, for instance by Newton-Raphson method:

$$t^{n+1} = t^n - \frac{z(t^n)}{\left(\frac{\partial z}{\partial t^n}\right)} \tag{10}$$

The value of t_0 found by Eq. (10) is then inserted in the remaining two $x(t)$ and $y(t)$ thus obtaining $\bar{r}_0$. Extending the problem to the general case of B bounded by a plane with arbitrary orientation, Eq. (8) becomes:

$$t_0 \rightarrow \bar{\omega}_p \bullet [\bar{r}(t_0) - \bar{r}_p] = 0 \tag{11}$$

with $\bar{\omega}_p$ the vector normal to the plane and $\bar{r}_p$ a point of the plane. Therefore, the recurrence equation to the search of the intersection point between the cubic spline and the plane is:

$$t^{n+1} = t^n - \frac{\bar{\omega}_p \bullet [\bar{r}(t^n) - \bar{r}_p]}{\bar{\omega}_p \bullet \left(\frac{\partial \bar{r}}{\partial t^n}\right)} \tag{12}$$

The new boundary node so found is added to the node list $\{P\}$ and the connectivity index of the crossing element is updated accordingly.

3.5 Computing the allowable thickness

As previously mentioned, the combined bending moments generated during the forming process of post formed grid shells, imposes the laths cross-sectional size to be designed under a certain limit value which automatic assessment is performed by running a two-step form finding analysis with an initial "assumed" value h_0 of the laths cross-sectional height. At completion of the analysis, a h^{n+1} value is computed and the DR analysis left to run fewer iterations, in order to obtain the new equilibrium for the effect of the updated stiffness term I_x. The process is repeated until the h value obtained corresponds to a desired limit bending stress ratio: According to Eurocode 5 Part 1-1 [19] (EC5) the following (EC5 6.11 and 6.12) relations apply for combined bending:

$$\frac{\sigma_x}{f_m} + k_m \frac{\sigma_y}{f_m} \le 1.0 \quad ; \quad k_m \frac{\sigma_x}{f_m} + \frac{\sigma_y}{f_m} \le 1.0 \tag{13}$$

Therefore, assuming a limit stress ratio equal to 1.0 but introducing a modification factor k_m = 0.7 for rectangular sections to take into account the variation of material properties and stress redistribution [20] (wood shows a plastic behaviour at compression failure point, while under tension a brittle failure mode occurs). Indicating with $\sigma_j^{6.11}$ and $\sigma_j^{6.12}$ the bending stress ratios obtained by Eqs. (13) for the generic jth element, we assume that for a given equilibrium configuration (at completion of the form finding analysis) the resulting maximum stress ratios $\sigma_{\max}^{6.11}$ and $\sigma_{\max}^{6.12}$ are represented by the values of two functions, whose argument h was set to a certain value h_0.

$$g(h_0) = \sigma_{\max}^{6.11} \quad ; \quad q(h_0) = \sigma_{\max}^{6.12} \tag{14}$$

Therefore, our aim is computing the value $h_{\text{allowable}}$ of the variable h such that one of the two $g(h)$ and $q(h)$ is equal to 1.0 while the other one is less that the unity. Calling the moment-stress relations:

$$\sigma_x = \frac{hM_x}{2I_x} \quad ; \quad \sigma_y = \frac{bM_y}{2I_y} \tag{15}$$

Thus, substituting Eqs. (15) into Eqs. (13) then, by rearranging, Eqs. (14) become:

$$\begin{aligned} g(h) &= \max\left(\frac{hM_{j,x}}{2I_x f_m} + k_m \cdot \frac{bM_{j,y}}{2I_y f_m} - 1\right) \\ f(h) &= \max\left(k_m \cdot \frac{hM_{j,x}}{2I_x f_m} + \frac{bM_{j,y}}{2I_y f_m} - 1\right) \end{aligned} \tag{16}$$

Accordingly, the problem is reduced to finding the roots of the $g(h)$ and $q(h)$ functions, which can be numerically solved by Newton-Raphson method:

$$h^{n+1} = \min\left\{\begin{matrix} h^n - \frac{g(h^n)}{\left(\frac{\partial g}{\partial h^n}\right)} \\ h^n - \frac{q(h^n)}{\left(\frac{\partial q}{\partial h^n}\right)} \end{matrix}\right\} \tag{17}$$

4 CALCULATION

4.1 Elastica

As in [8, 17] the developed six DoF DR formulation is tested for the bi-dimensional case, against the analytical solution of an initially straight elastic rod pinned at its end. The load values of P corresponding to the four shapes are obtained according to Timoshenko and Gere [21] as: $P = (K^2 \cdot EI)L^{-2}$ with the *complete elliptic integral of the first kind* (K) computed up to the 10th decimal place in order to maintain high accuracy of the analytic solution. An axial stiffness EA=100.0MN and bending stiffness EI=*100.0*kNm^2 were set. The rod's length is 10.0m. For each of the four buckled states, five DR analyses with increasing number of elements (20 up to 36) were performed. The analyses were stopped when the following inequality limit was reached: $\max|\bar{R}_i| \le$9.5e-6P. The numerical x displacement of the rod's right-end node and y

displacement of the mid-span node are compared to the corresponding analytical values in terms of error percentage and summarized in Figure 3.

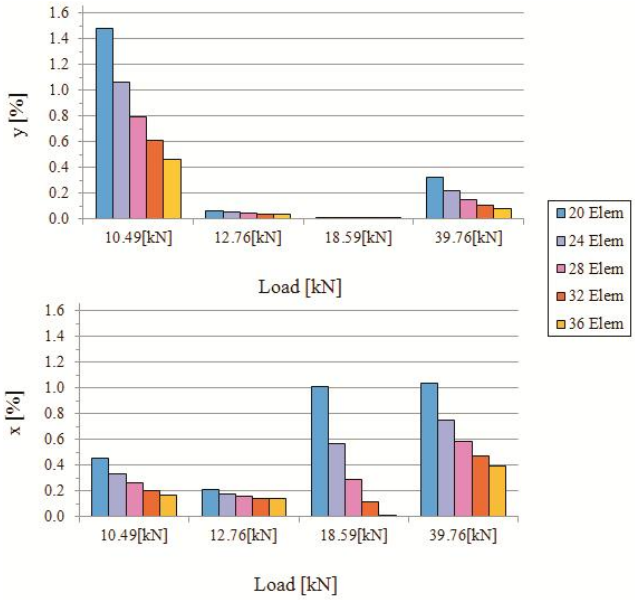

Figure 3: *Numerical displacements error at different discretization values.*

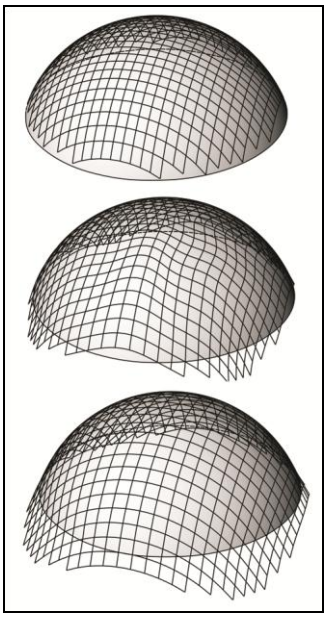

Figure 4: *Form finding of a spherical dome.*

4.2 Spherical dome

This example provides a description of the developed method with a practical application to the form finding of a grid shell dome. The reference surface is described by the equation of a sphere having radius of 11.0m and its centre coinciding with the global axes origin. The subspace of interest B is defined by $z \geq 4.582$m so that each grid node which z coordinate at time t is lower than such value, it is not constrained to the surface. Accordingly, the part of reference surface contained in B configures a spherical cap with a span of 20.0m and circa 6.4m high (see Figure 4). The unstressed length L_0 of the two-way grid is set to 1.0m. The mesh obtained with the cutting algorithm previously described, can be used to find the corresponding flat grid by "relaxing" it on a planar surface. In fact, although geometrically different, the two meshes have the same topology.

4.3 Corrugated barrel vault

This example aims to test the Newton-Raphson algorithm, described in subsection **3.5** (for cross-section optimization) by computing the geometry of a real post formed timber grid shell and comparing the resulting outputs in terms of stress ratios. The reference surface is modelled in such a way to replicate the overall shape of the Downland grid shell. Writing the reference surface function $f(x,y,z)=0$ in the form $f(x,y)=z$, we have:

$$z = -\cosh\left(\frac{x}{2.55}\right)+\cosh\left(\frac{x}{4.1}\right)\cdot\cos\left(\frac{y}{3}\right)-\left(\frac{x^2}{50}+\frac{y^2}{665}\right)+9.55 \quad (18)$$

Accordingly, the global (x, y) plane coincides with the ground floor level of the real structure which longitudinal axis is directed along the y global direction. Hence, the subspace of interest B is defined by: ($z \geq 0.0m$) and $(-25.0m \leq y \leq 25.0m)$. The resulting corrugated barrel vault is 50.0m long, with a varying width of 12.5m to 16.0m, while the height varies from 9.5m at the central hump to circa 7.4m at the saddles [7].

According to Harris et al [4] the timber specimens were graded as D30 of the BS-EN-338 strength classification [22], for which a mean modulus of elastic parallel to the grain ($E_{0,\ mean}$) of 11.0kN/mm^2 is given. Such value is estimated from tests on timber population at a temperature of 20°C and relative humidity of 65%. In these environmental conditions the moisture content (MC) of wood in general does not exceed 12% (dry timber) while the green oak used for the Downland grid shell construction had a MC up to 65% [4]. For values of MC over the fibre saturation point (≈27%) a reduction in stiffness and strength occurs. In order to take this reduction into account, a (E_{dry}/E_{green}) ratio of 1.3 [23] is considered to derive a (reasonable) value of elastic modulus:

$$E = \frac{E_{0,mean}}{1.3} = 8.46(kN/mm^2) \quad (19)$$

which is used to compute the elements internal reactions, thus the out of balance forces $\overline{R}_i^t$ and moments $\overline{H}_i^t$. For strength, the five-percentile value of 30.0N/mm^2 given by BS EN 338 was considered. A mean value of 0.69kNmm^2 [22] is set for the transverse shear modulus. The initial rectangular mat shape [4] is preserved during the form

finding analysis by constraining the vertical displacements of the boundary nodes of the flat mat's longer side.

For a lath cross-section of 50.0mm x 35.0mm the resulting stress ratios $\sigma_{\max}^{6.11}$ and $\sigma_{\max}^{6.12}$ at analysis completion are found to be 100.8% and 99.1% respectively, thus correctly "forecasting" the allowable-thickness, max-stress-ratio functions.

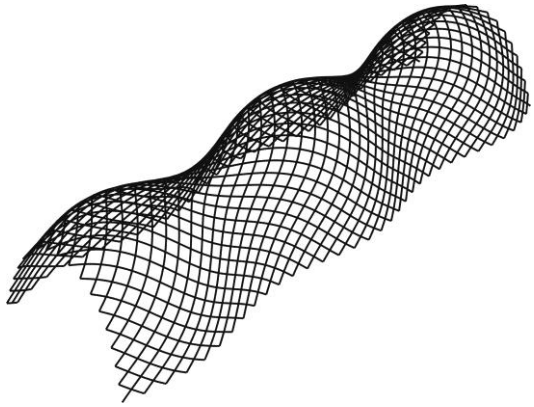

Figure 5: *Corrugated barrel vault.*

5 CONCLUSIONS

The work presented in this paper has aimed to facilitate the design of post formed grid shells, with particular attention on the use of timber. A numerical framework is developed to address a range of problems at various design stages, including form finding, structural analysis and assembly definition (flat mat geometry). The accompanying numerical tests demonstrated the framework reliability. The preliminary tests on the single rod case showed a high accuracy level of the six DoF DR formulation in the estimation of the load-displacement functions as well as the Newton-Raphson algorithm for cross-section optimization.

ACKNOWLEDGEMENT

The Centre for Timber Engineering (CTE) and the school of Engineering and Built Environment at Edinburgh Napier Edinburgh University are greatly acknowledged for providing financial support for this research.

REFERENCES

[1] R. Harris, Design of timber gridded shell structures, Proceedings of the ICE Structures and Buildings 164 (2) (2011) 105-116.

[2] C. Pirazzi, Y. Weinand, et al., Geodesic lines on free-form surfaces: optimized grids for timber rib shells, in: Proc. World Conference on Timber Engineering, Vol. 7, 2006.

[3] E. Happold, W. Liddell, Timber lattice roof for the Mannheim Bundesgartenschau, The structural engineer 53 (3) (1975) 99-135.

[4] R. Harris, J. Romer, O. Kelly, S. Johnson, Design and construction of the Downland gridshell, Building Research & Information 31 (6) (2003) 427-454.

[5] R. Harris, S. Haskins, J. Roynon, The Savill garden gridshell: design and construction, The Structural Engineer 86 (17) (2008) 27-34.

[6] S. Pone, B. D'Amico, S. Colabella, B. Parenti, D. Lancia, A. Fiore et al, Construction and form-finding of a post-formed timber grid-shell, in: Structures and Architecture. Concept, Applications and challenge, 2013, pp. 245-252.

[7] O. Kelly, R. Harris, M. Dickson, J. Rowe, The construction of the Downland gridshell, The Structural Engineer 79 (17) (2001) 25-33.

[8] C. Douthe, O. Baverel, J.-F. Caron, Form-finding of a grid shell in composite materials, Journal-International association for shell and Spatial Structures 150 (2006) 53.

[9] L. Bouhaya, O. Baverel, J.-F. Caron, mapping two-way continuous elastic grid on an imposed surface: Application to grid shells, in: Proc. 50th International IASS Symposium, Valencia, Editorial de la Universitat Politecnica de Valencia., 2010.

[10] J.M. Li, J. Knippers, Form-finding of grid shells with continuous elastic rods, in: Proc. of the International Symposium of the IABSE-IASS Symposium, London, UK, Vol. 35, 2011.

[11] M. Kuijvenhoven, P. Hoogenboom, Particle-spring method for form finding grid shell structures consisting of flexible members, Journal of the International Association for Shell and Spatial Structures 53 (1) (2012) 31-38.

[12] S. Pone, S. Colabella, B. D'Amico, D. Lancia, A. Fiore, B. Parenti, Timber post-formed gridshell: Digital form-finding / drawing and building tool, in: Proc. of the International IASS Symposium, Wroclaw, Poland, 2013.

[13] R. Harris, B. Gusinde, J. Roynon, Design and construction of the pods sports academy, Scunthorpe, England, in: World Conference of Timber Engineering, 2012, pp. 510-517.

[14] A. Day, An introduction to dynamic relaxation, The engineer 219 (1965) 218-221.

[15] J. R. H. Otter, A. C. Cassell, R. E. Hobbs, et al., Dynamic relaxation, in: ICE Proceedings, Vol. 35, Thomas Telford, 1966, pp. 633-656.

[16] W. J. Lewis, Tension structures: form and behaviour, Thomas Telford, 2003.

[17] S. Adriaenssens, M. Barnes, Tensegrity spline beam and grid shell structures, Engineering structures 23 (1) (2001) 29-36.

[18] M. R. Barnes, S. Adriaenssens, M. Krupka, A novel torsion/bending element for dynamic relaxation modelling, Computers & Structures 119 (2013) 60-67.

[19] BS EN 1995-1-1:2004+A1:2008. Eurocode 5: Design of timber structures - Part 1-1: General - Common rules and rules for buildings, British Standards Institution.

[20] J. Porteous, A. Kermani, Structural timber design to Eurocode 5, 2nd edition, John Wiley & Sons, 2013.

[21] S. P. Timoshenko, J. M. Gere, Theory of elastic stability, McGraw-Hill, 1961.

[22] BS EN 338:2009. Structural timber - Strength classes, British Standards Institution.

[23] ASTM D2555-06. Standard Practice for Establishing Clear Wood Strength Values, American Society for Testing and Materials, 2006.